

1
2
3
4
5
6
7
8
9
10
11
12
13
14
15
16
17
18
19
20
21
22
23

Journal of Geophysical Research: Solid Earth

Supporting Information for

Compression of a multiphase mantle assemblage: Effects of undesirable stress and stress annealing on the iron spin-state crossover in ferropericlase

Konstantin Glazyrin^{1,2}, Nobuyoshi Miyajima³, Jesse S. Smith⁴, Kanani K.M. Lee¹

¹Department of Geology & Geophysics, Yale University, PO Box 208109, New Haven, CT, 06520-8109 USA; ²FS-PE Group, DESY Deutsches Elektronen-Synchrotron Ein Forschungszentrum der Helmholtz-Gemeinschaft, D-22607 Hamburg, Germany; ³Bayerisches Geoinstitut, Universität Bayreuth, D-95440 Bayreuth, Germany; ⁴High Pressure Collaborative Access Team, Geophysical Laboratory, Carnegie Institution of Washington, Argonne National Laboratory, Argonne, IL 60439, USA

Contents of this file

Figures (S1-S6), Table S1 and additional evidence supporting our discussion given in the manuscript.

Introduction

Below we discuss previous literature data describing spin transition in ferropericlase with focus on critical pressure of the transition (Chapter 1).

In addition to that we present characterization of the material by various techniques (Chapter 2).

Finally, we present our estimation on Au-Pd alloy equation of state (Chapter 3).

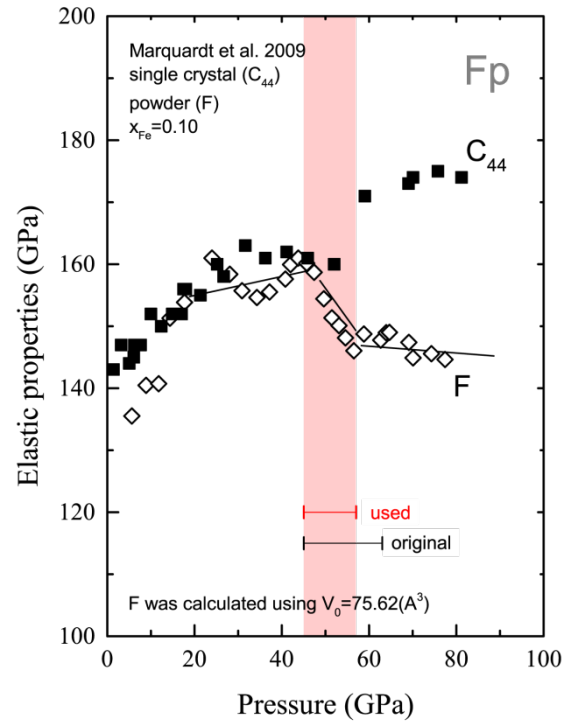
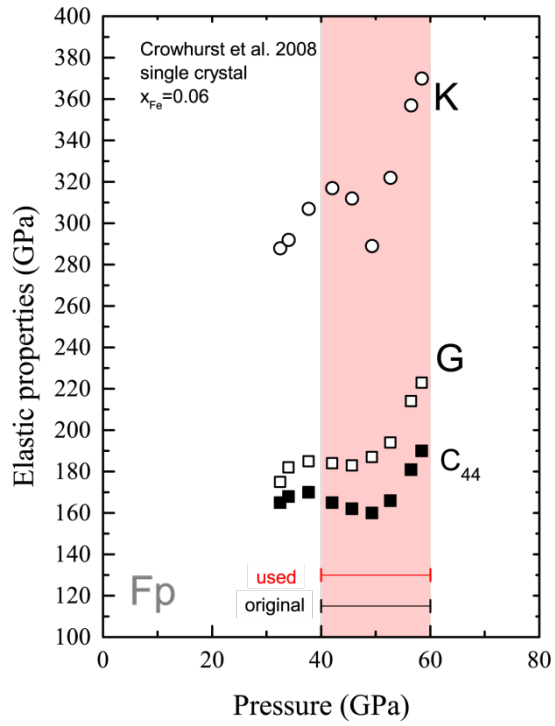
24

25 **1 FERROPERICLASE ($\text{Mg}_{1-x}\text{Fe}_x\text{O}$ - Fp) IRON SPIN-STATE CROSSOVER**

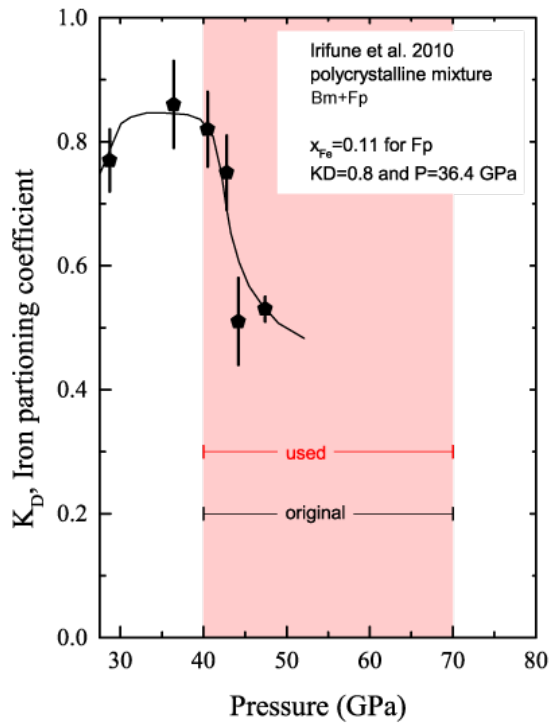
26 Below we present a comparative analysis of ambient single crystal and powder data for Fp
27 phase with different concentrations of iron. Special attention is dedicated to imposing objective
28 constraints on the observed iron spin-state crossover critical pressures indicating start (P_{SSC}) and
29 end of the crossover (Figure S1).

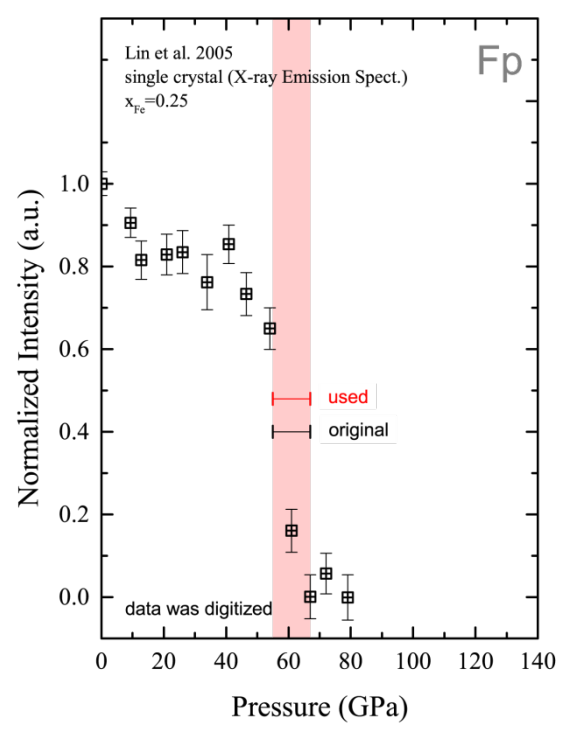
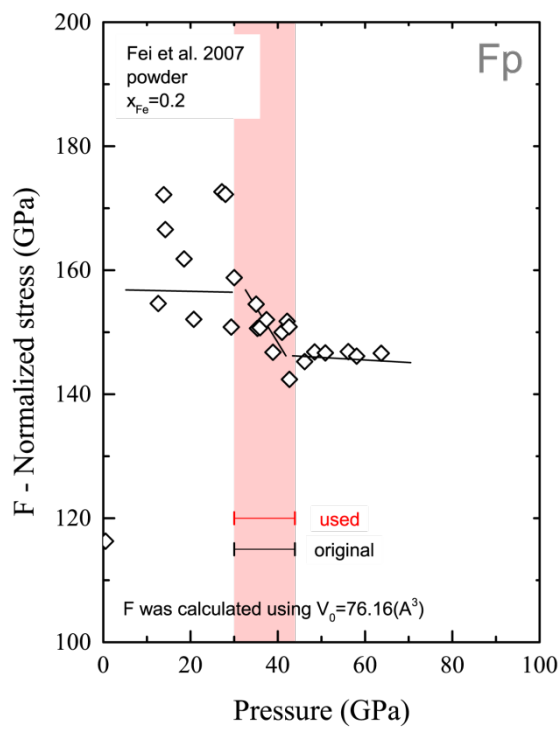
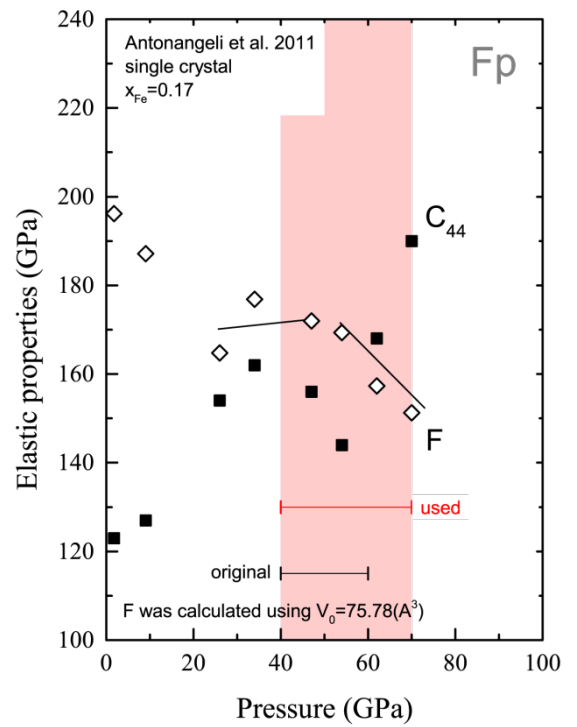
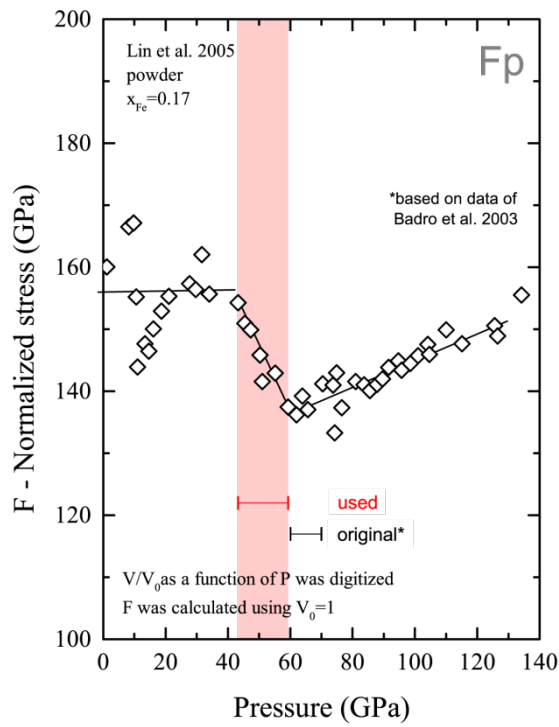
30 All data, unless specified in a figure caption, is plotted according to original data given in
31 publications or in corresponding Supplementary Information. We increased reported pressure
32 range for data of Antonangeli et al. 2011 after comparing the data with Marquardt et al. 2009 and
33 Crowhurst et al. 2005. From the analysis of C_{44} compression behaviours, we find it clear that 70
34 GPa point from Antonangeli et al 2011 is on the edge of Fp LS state and that the material may
35 have residual contribution from HS state. We changed the originally proposed range for $x=0.17$
36 [Lin et al., 2005]. The original range for spin-state crossover (60-70 GPa) was proposed relying
37 on conclusions from [Badro et al., 2003], and thus, as we believe the actual transition range was
38 misinterpreted. Indeed, in the original publication Badro et al. [2003] detect changes of the XES
39 spectra from 49 to 75 GPa, which we will use in our analysis. Most of other suggested
40 corrections are based on comparison of literature data and $F-f_E$ plots, modified below into F-P
41 plots for clarity.

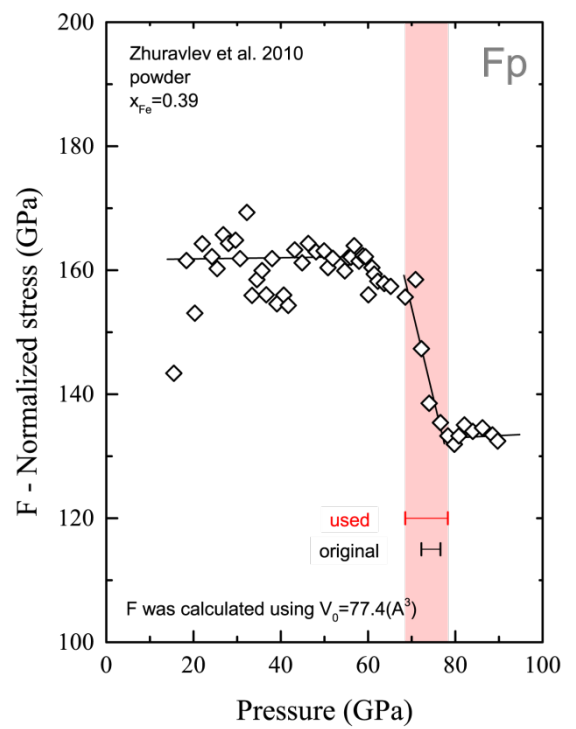
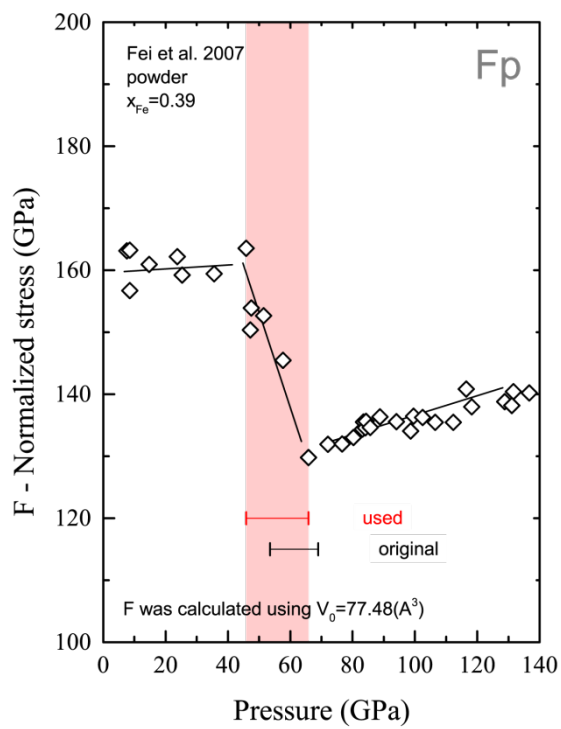
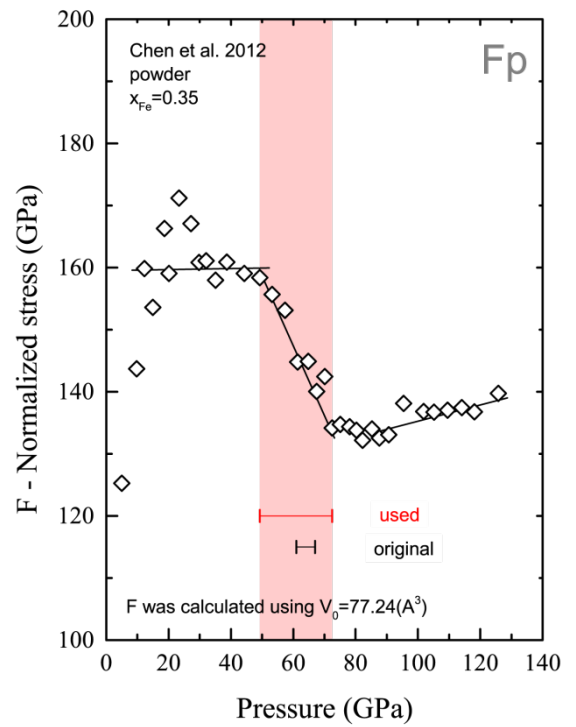
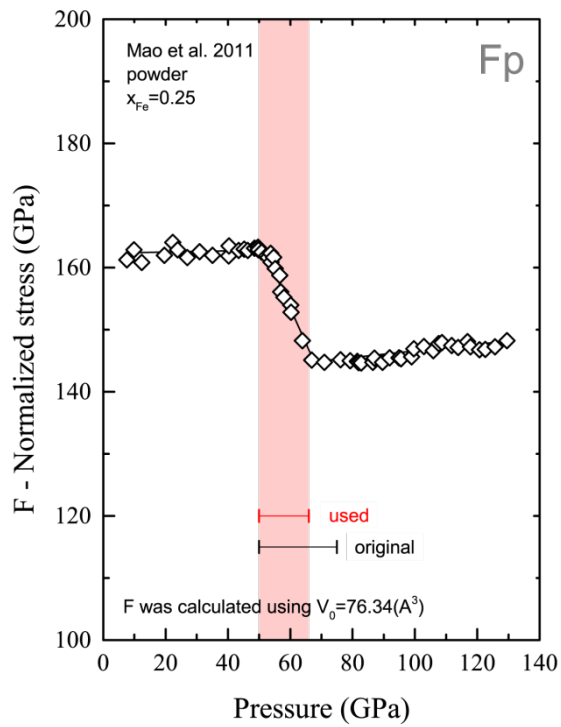
42 Inconsistencies in the iron spin-state crossover phase diagram can be attributed to low
43 number of points, high scatter of points. However, in our paper we address a major problem,
44 when starting pressures and pressure ranges for spin-state crossover are inconsistent for similar
45 compositions.



46
47
48
49







50
51

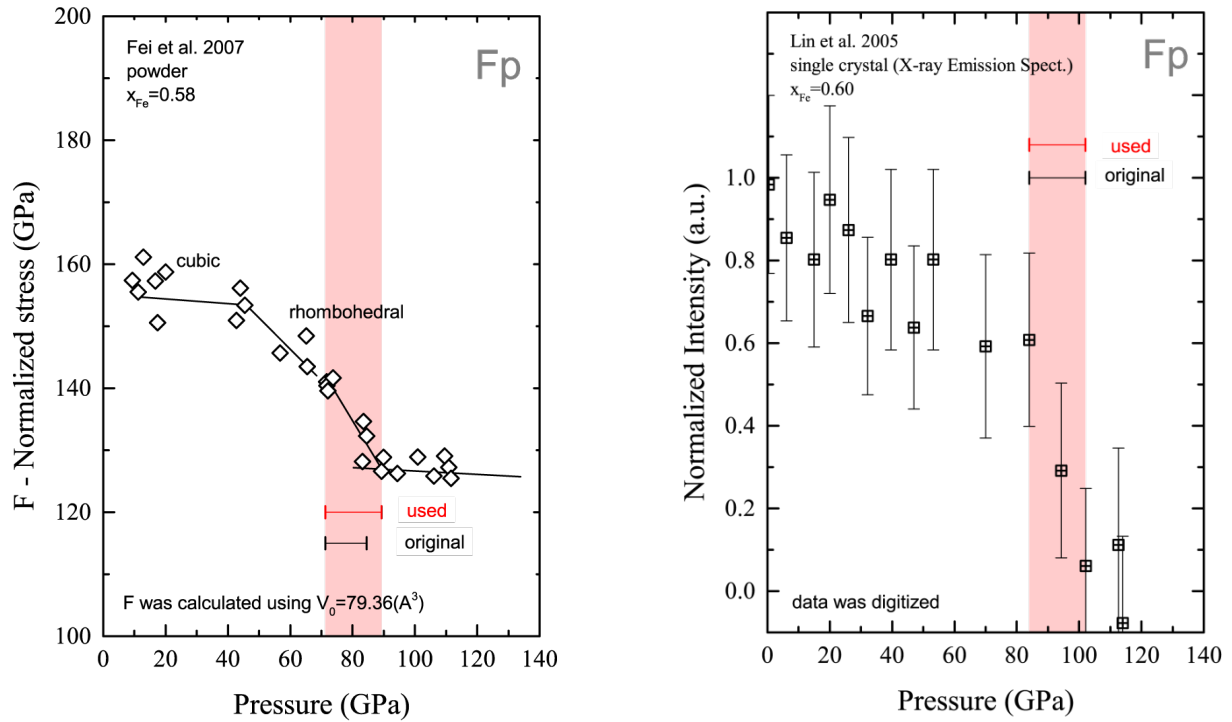


Figure S1. Literature data used for construction of Fp iron spin state crossover phase diagram. Unless otherwise stated, the data was taken from tables provided in the publications main text or in the corresponding Supplementary Information. We use the following notations: F – Normalized stress, P – pressure, V - volume, K – bulk modulus, G – shear modulus, C_{44} – crystal lattice elastic constant and $K_D = (\text{Fe/Mg})_{\text{Mg-Bm}} / (\text{Fe/Mg})_{\text{Mw}}$ is the iron partitioning coefficient between magnesium silicate perovskite (Bm) and Fp. The data on iron partitioning coefficient K_D was taken from [Irfune *et al.*, 2010]. For data $x=0.58$ of [Fei *et al.*, 2007a] we feature material phase transition from cubic to rhombohedral phase occurring at lower pressures compared with HS-LS crossover. Labels placed on figures describe iron concentration in Fp. Red shading together with region highlighted by horizontal red bar labeled as ‘used’ indicates iron spin state crossover used for construction of the phase diagram presented in the manuscript body. Horizontal black bar indicates pressure range originally suggested in the publications. Black lines are the eye guides.

53 **2 SAMPLE PREPARATION AND CHARACTERIZATION**

54 Below we show a scanning electron microphotograph of the synthesized K1297 material.

55 Image was obtained in the center of the capsule using a backscattered electrons sensor (K.E.

56 Developments) installed on XL30 Scanning Electron Microscope (SEM) at Yale University.

57 Brighter and darker areas correspond to iron rich magnesium ferropericlase phase (Fp) and

58 iron poor magnesium silicate perovskite phases (Bm), respectively.

59

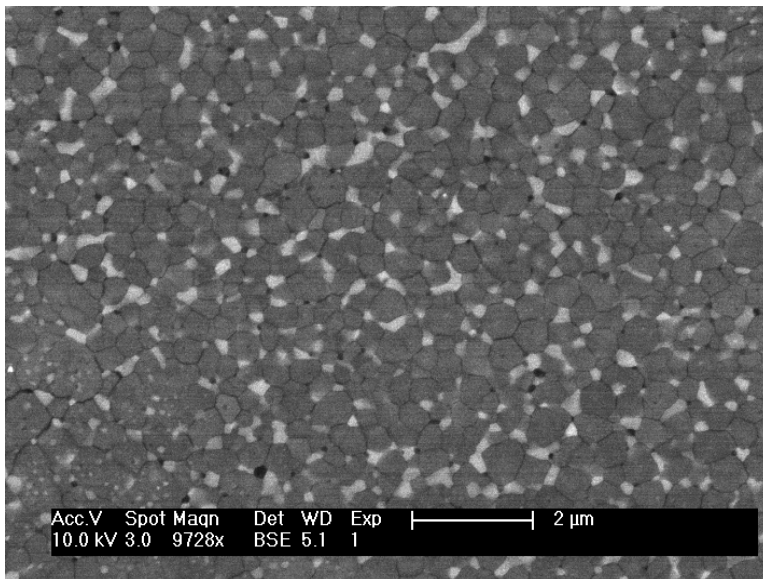


Figure S2. SEM image of the prepared material (K1297). High contrast image collected in backscattered electrons mode features two phases quenched from high pressure - high temperature conditions, namely, Bm (dark gray) and Fp (light grey). Higher brightness of Fp grains is a result of higher Fe concentration.

60

61 We present additional information from our TEM EELS study and Mössbauer spectroscopy

62 study on sample characterization in the figures and table shown below.

63

64

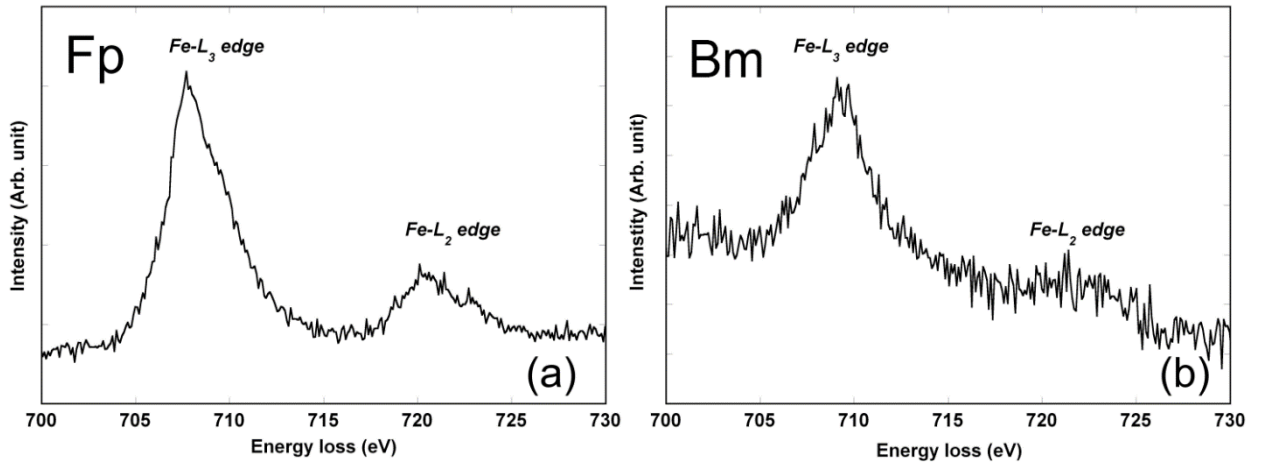


Figure S3 Fe $L_{2,3}$ -edge ELNES spectra of Fp grain (a) and Bm grain (b) found in K1297 sample.

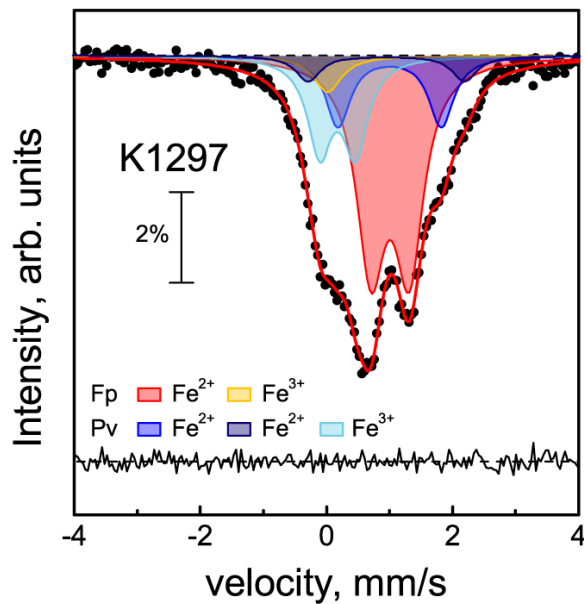


Figure S4. Mössbauer spectrum of K1297 sample collected at ambient conditions. Data points are black, and red line passing through the points represents the fit. We highlight the following contributions. Red and yellow shaded area correspond to ferrous iron and ferric iron incorporated into Fp, respectively. Blue, dark blue and light blue areas correspond to two ferrous iron positions and one ferric iron position in Bm, respectively. Black line at the bottom features the fit residuals.

65
66
67
68
69

Table S1. Mössbauer parameters for sample K1297. Isomer shift (IS) values are given relative to the iron foil. QS represents quadrupole splitting. Values marked with stars were fixed or constrained during the fit of the spectrum. Area of the yellow subspectrum was constrained to 9% of the red subspectrum area during the fit and is identified by an asterisk. At the same time isomer shift of yellow subspectrum was fixed to 0.13 mm/s. This is a reasonable value for ferric iron in Fp [Otsuka *et al.*, 2010] synthesized in the multianvil at ~1800 K.

Subspectrum	Phase	IS, mm/s	QS, mm/s	Area, %
Red	Fp Fe ²⁺	1.12(1)	0.61(1)	52.8(19)
Yellow	Fp Fe ³⁺	0.13		4.8*
Blue	Bm Fe ²⁺	1.06(1)	2.48(7)	5.7(9)
Dark Blue	Bm Fe ²⁺	1.11(1)	1.63(5)	15.9(18)
Light blue	Bm Fe ³⁺	0.29(1)	0.57(2)	20.8(9)

71

72 3 AU-PD EQUATION OF STATE

73 In our study we employed (75wt% Au and 25wt% Pd) as capsule material in multianvil
 74 synthesis from glass material. Composition of the material is confirmed by x-ray diffraction and
 75 energy dispersive x-ray spectroscopy mode of scanning electron microscope XL30. Finite
 76 amount of Au-Pd was incorporated into synthesized K1297 material and, respectively, into S2
 77 sample.

78 In order to exploit this material as an X-ray diffraction pressure standard, we need to know
 79 the relations connecting its unit cell volume and pressure, for example, its Birch-Murnaghan
 80 equation of state. Assuming an fcc cubic lattice and ideal solid solution [Okamoto and
 81 Massalski, 1985], we can estimate isothermal bulk modulus of our Au-Pd alloy through Voigt-
 82 Reuss-Hill (VRH) and Hashin and Shtrikman bounds (HS) [Watt *et al.*, 1976]. The physical
 83 meaning of HS bounds corresponds to a case of ‘composite sphere assemblage’ justifying our
 84 approach. In order to calculate bulk modulus for the alloy, we need end-member ambient
 85 temperature parameters, namely, isothermal bulk modulus (K_0), shear modulus (G), volume (V_0)
 86 and bulk modulus pressure derivative (K'). We used the following parameters for gold:

87 $K_0^{Au}=167$ GPa, $V_0^{Au}= 67.85 \text{ \AA}^3$, $K^{Au}=5.77$, $G^{Au}=27$ GPa [Duffy et al., 1999; Fei et al., 2007b],
 88 and the following for palladium: $K_0^{Pd}=193$ GPa, $V_0^{Pd}=58.88 \text{ \AA}^3$, $K^{Pd}=5$, $G^{Pd}=53.3$ GPa [Rayne,
 89 1960; Okamoto and Massalski, 1985; Weller et al., 1991].

90 In figures below we show values of bulk modulus and variation of crystallographic unit cell
 91 for Au-Pd alloys as a function of Pd content at ambient conditions.

92 We calculate K_0^{Au-Pd} using Hashin and Shtrikman equations and show the corresponding
 93 values (Figure S5). Volume fractions of Au and Pd end members are calculated according to a
 94 linear approximation of Au and Pd contribution to the Au-Pd alloy volume. This approach is
 95 justified by very small deviation of Au-Pd unit cell parameters from the Vegard's rule and by
 96 insignificant error introduced by using the assumption that volume of the alloy is a linear
 97 function of Au and Pd concentrations. For pressure determination using Au-Pd alloy as a
 98 standard, we compute the following parameters: $K_0^{Au-Pd}=176.5$ GPa, $V_0^{Au-Pd}= 64.29 \text{ \AA}^3$,
 99 $K^{Au-Pd}=5.5$.

100

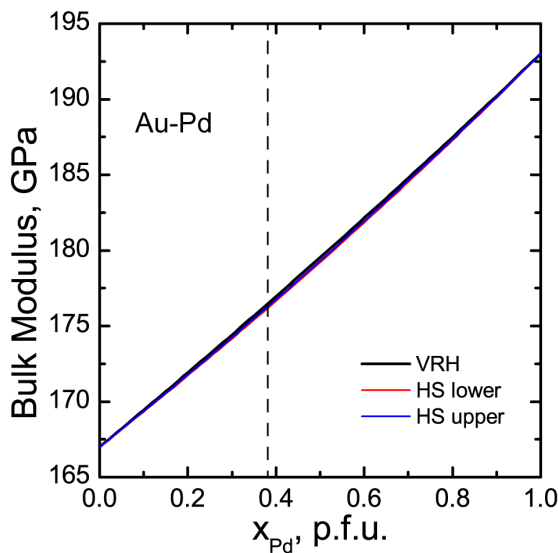


Figure S5. Variation of K_0^{Au-Pd} as a function of Pd concentration calculated within VRH, HS approximations. Vertical dashed line corresponds to our 75wt% Au and 25wt% Pd composition. Note similarity of the values calculated using Hashin-Shtrikman (HS) and Voigt-Reuss-Hill (VRH) approaches.

101

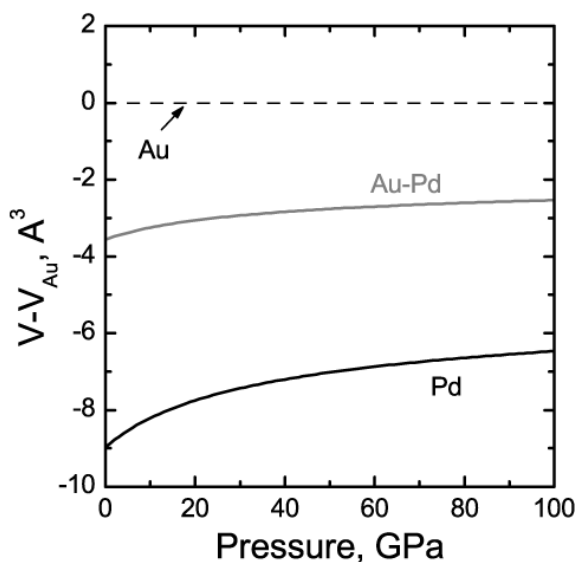


Figure S6. Relative difference of Au-Pd (75wt% Au and 25wt% Pd), Pd and Au unit cell volumes as a function of pressure. We take pure Au as a reference (dashed line).

102

103 REFERENCES

- 104 Badro, J., G. Fiquet, F. Guyot, J.-P. Rueff, V. V. Struzhkin, G. Vankó, and G. Monaco (2003),
 105 Iron Partitioning in Earth's Mantle: Toward a Deep Lower Mantle Discontinuity, *Science* (80).,
 106 300(5620), 789–791, doi:10.1126/science.1081311.
- 107 Duffy, T. S., G. Shen, J. Shu, H.-K. Mao, R. J. Hemley, and A. K. Singh (1999), Elasticity, shear
 108 strength, and equation of state of molybdenum and gold from x-ray diffraction under
 109 nonhydrostatic compression to 24 GPa, *J. Appl. Phys.*, 86(12), 6729
- 110 Fei, Y., L. Zhang, A. Corgne, H. Watson, A. Ricolleau, Y. Meng, and V. Prakapenka (2007a),
 111 Spin transition and equations of state of (Mg, Fe)O solid solutions, *Geophys. Res. Lett.*, 34(17)
- 112 Fei, Y., A. Ricolleau, M. Frank, K. Mibe, G. Shen, and V. Prakapenka (2007b), Toward an
 113 internally consistent pressure scale, *Proc. Natl. Acad. Sci.*, 104(22), 9182–9186
- 114 Irifune, T., T. Shinmei, C. A. McCammon, N. Miyajima, D. C. Rubie, and D. J. Frost (2010),
 115 Iron partitioning and density changes of pyrolite in Earth's lower mantle., *Science*, 327(5962),
 116 193–5
- 117 Lin, J.-F., V. V. Struzhkin, S. D. Jacobsen, M. Y. Hu, P. Chow, J. Kung, H. Liu, H.-K. Mao, and
 118 R. J. Hemley (2005), Spin transition of iron in magnesiowüstite in the Earth's lower mantle,
 119 *Nature*, 436(7049), 377–380
- 120 Okamoto, H., and T. B. Massalski (1985), The Au–Pd (Gold–Palladium) system, *Bull. Alloy
 121 Phase Diagrams*, 6(3), 229–235

- 122 Otsuka, K., C. a. McCammon, and S. Karato (2010), Tetrahedral occupancy of ferric iron in
123 (Mg,Fe)O: Implications for point defects in the Earth's lower mantle, *Phys. Earth Planet. Inter.*,
124 *180*(3-4), 179–188
- 125 Rayne, J. (1960), Elastic Constants of Palladium from 4.2-300°K, *Phys. Rev.*, *118*(6), 1545–1549
- 126 Watt, J. P., G. F. Davies, and R. J. O'Connell (1976), The elastic properties of composite
127 materials, *Rev. Geophys.*, *14*(4), 541
- 128 Weller, M., J. Diehl, and H. E. Schaefer (1991), Shear modulus and internal friction in
129 nanometre-sized polycrystalline palladium, *Philos. Mag. A*, *63*(3), 527–533
- 130